Hindawi
Mathematical Problems in Engineering
Volume 2018, Article ID 2804123, 19 pages
https://doi.org/10.1155/2018/2804123

Research Article

Thermoelastic Analysis of Rotating Functionally Graded Truncated Conical Shell by the Methods of Polynomial Based Differential Quadrature and Fourier Expansion-Based Differential Quadrature

Aref Mehditabar,[1] **Gholam H. Rahimi**,[1] **and Kerameat Malekzadeh Fard**[2]

[1]*Department of Mechanical Engineering, Tarbiat Modares University, Tehran, Iran*
[2]*Department of Structural Analysis and Simulation, Aerospace Research Institute, Malek-Ashtar University of Technology, Tehran, Iran*

Correspondence should be addressed to Aref Mehditabar; a.mehditabar@modares.ac.ir

Received 20 December 2017; Revised 18 February 2018; Accepted 28 February 2018; Published 20 May 2018

Academic Editor: Francesco Tornabene

This paper focuses on the three-dimensional (3D) asymmetric problem of functionally graded (FG) truncated conical shell subjected to thermal field and inertia force due to the rotating part. The FG properties are assumed to be varied along the thickness according to power law distribution, whereas Poisson's ratio is assumed to be constant. On the basis of 3D Green-Lagrange theory in general curvilinear coordinate, the fundamental equations are formulated and then two versions of differential quadrature method (DQM) including polynomial based differential quadrature (PDQ) and Fourier expansion-based differential quadrature (FDQ) are applied to discretize the resulting differential equations. The reliability of the present approach is validated by comparing with known literature where good agreement is reached using considerably few grid points. The effects of different mechanical boundary conditions, temperature fields, rotating angular speed, and shell thickness on the distributions of stress components and displacement in thickness direction for both axisymmetric and asymmetric cases are graphically depicted.

1. Introduction

Sharp discontinuity and delamination problems in monolithic laminated composite materials impelled scientists to come up with the idea of new class of advanced composite material, so-called functionally graded materials (FGMs). FGMs are characterized by smooth variations in material properties from one interface to other based on specific function. Mixture of ceramic phase with metal phase by gradual transition between two phases enables the materials to have the higher wear and thermal and corrosion resistances and avoids the resultant stress concentrations in traditional composite materials [1]. In many industrial applications, FG components are commonly exposed to thermal and mechanical load fields. Hence, determination of the optimum material gradient of FGMs has major rule on reduction of the produced stresses in structure. The papers corresponding to thermoelastic analysis of FGM because of the close concept to present work are brought here. Afsar and Go [2] developed finite element modelled for an axisymmetric rotating FG circular disk under thermoelastic field. Bayat et al. [3] analyzed the FG rotating disk with variable thickness under thermal, bending, and body loads. Peng and Li [4] presented thermoelastic problem of an FG hollow cylinder using Fredholm integral equations. Kiani [5] applied the surface elasticity theory of Gurtin and Murdoch to carry out the thermoelastic analysis of rotating FG nanoplate. Kar and Panda [6] focused on fully nonlinear and linear bending analysis of spherical FG panel under thermomechanical loadings. Eslami et al. [7] studied one-dimensional (1D) problem of a thick-walled FG hollow sphere subjected to thermomechanical loadings. Hosseini and Dini [8] presented analytical solution of thick-walled FG rotating cylinder under magneto-thermo-mechanical loadings. Natarajan et al. [9] employed the cell-based smoothed finite element method with discrete shear

gap technique to investigate the static and dynamic behavior of FG plates. Leu and Chien [10] studied thermoelastic behavior of FG rotating disk with variable thickness involving nonuniform heat source. Mehditabar et al. [11] investigated the magneto-thermoelastic analysis of FG truncated conical shell using DQM approach. Punera et al. [12] presented analytical solutions for thermoelastic analysis of laminated and FG sandwich open cylindrical shell. Xin et al. [13] discussed the thermoelastic responses of the thick-walled FG tube under thermal and mechanical load fields employing Voigt method. Prakash and Ganapathi [14] studied the asymmetric free vibration and thermoelastic stability of FG circular plates by employing finite element method. Based on Gren-Naghdi thermoelasticity theories and using Laplace and Fourier transforms the magneto-thermoelastic analysis of rotating medium was carried out by Kumra et al. [15]. Kordkheili and livani [16] proposed a semianalytical-numerical method to investigate the thermoelastic responses of the FG rotating disks with variable thickness and also in another work the thermoelastic analysis coupled with creep behavior [16] of the same problem was carried out by them. The thermoelastic behavior of rotating FG cylindrical shell with piezoelectric layers applying DQM technique was studied by Saadatfar and Aghaei-Khafri [17]. In their research, the material properties of FGM and FGMP (functionally graded piezoelectric) were assumed to be distributed according to exponential rule across radial direction. Eraslan and Akis [18] performed the elastic-plastic analysis of FG pressurized tube subjected to thermal load. Jabbari et al. [19] investigated the thermoelastic problem of the rotating thick FG cylindrical shell with material gradient in axial direction utilizing multilayer method (MLM). Chikh et al. [20] carried out nonlinear postbuckling analysis of symmetric FG plate under thermomechanical loads. Behravan Rad [21] investigated thermoelastic behavior of FG annular plate resting on a hybrid elastic foundation undergoing asymmetric mechanical load and axial temperature gradient. Isavand et al. [22] studied dynamic analysis of FG steel (FGS) cylindrical panel employing hybrid Fourier series expansion-Galerkin finite element method, Newmark. Mehditabar [23] modelled 3D FG truncated conical shell immersed in magneto-thermomechanical fields.

In this paper 3D asymmetric thermoelastic analysis of rotating FG truncated conical shell under temperature gradient through thickness and centrifugal load duo to rotation of the shell is investigated. The variations of material properties are assumed to be varied along the thickness according to power law rule, whereas Poisson's ratio is supposed to be constant. Due to intrinsic complexity of existing equations, two versions of DQM technique including PDQ and FDQ in conjunction with Newton-Raphson iteration technique are employed to obtain the numerical results. The validity of the present approach is proved by comparing with that published literature that the good consistency using considerably few grid points is achieved. In this study, the sensitivities of displacement and stress components to different values of thermal loading, thickness of shell, rotating angular speed, and boundary conditions under both axisymmetric and asymmetric loading conditions are graphically plotted and discussed.

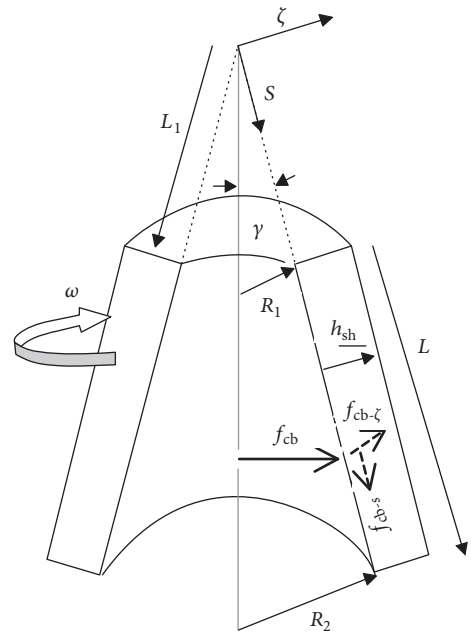

Figure 1: Physical model and system coordinates of the truncated conical shell.

2. Governing Equations

The FG truncated conical shell with the origin of the coordinate at vertex of whole cone, as illustrated in Figure 1, is considered. According to Figure 1, the set of orthogonal curvilinear coordinates s, θ, and ζ lie on meridian, circumferential, and thickness directions, respectively. The thickness of the shell is defined as h_{sh}, R_1, and R_2 indicate the inner and outer radii of the cone at its small and large edge, respectively, L_1 denotes distance from the vertex to its small edge, L is length of the cone along the generator, γ determines the semivertex angle, and ω is rotating angular speed. Moreover, f_{Cb}, $f_{Cb\text{-}\zeta}$, and $f_{Cb\text{-}s}$ indicate the total centrifugal force and its components along ζ and s directions, respectively.

In this study, the elastic modulus, heat conductivity and coefficients of thermal expansion are assumed to be varied only along the thickness direction according to the selected power law function as follows [11]:

$$\begin{aligned} E(\zeta) &= E_0\left(1+\frac{\zeta}{h_{sh}}\right)^n, \\ \alpha(\zeta) &= \alpha_0\left(1+\frac{\zeta}{h_{sh}}\right)^n, \\ K(\zeta) &= K_0\left(1+\frac{\zeta}{h_{sh}}\right)^n, \\ \upsilon(\zeta) &\simeq \upsilon. \end{aligned} \tag{1}$$

E_0, α_0, and K_0 are the elastic modulus, coefficient of thermal expansion, and thermal conductivity at the inner surface of shell, respectively, and also n represents the FG inhomogeneity constant. Consider u, v, and w as corresponding displacement components in s, θ, and ζ, respectively; the

relationships between strain and displacement based on 3D elasticity formulations in the conical coordinate are expressed as [25]

$$\begin{aligned}
\varepsilon_{ss} &= \frac{\partial}{\partial s}u,\\
\varepsilon_{\theta\theta} &= Z\left(\left(\frac{\partial}{\partial\theta}v\right) + w\cos(\gamma) + u\sin(\gamma)\right),\\
\varepsilon_{\zeta\zeta} &= \frac{\partial}{\partial\zeta}w,\\
\varepsilon_{\theta\zeta} &= Z\left(\left(\frac{\partial}{\partial\theta}w\right) - \cos(\gamma)\,v\right) + \left(\frac{\partial}{\partial\zeta}v\right),\\
\varepsilon_{s\theta} &= Z\left(\left(\frac{\partial}{\partial\theta}u\right) - \sin(\gamma)\,v\right) + \left(\frac{\partial}{\partial s}v\right),\\
\varepsilon_{s\zeta} &= \left(\frac{\partial}{\partial\zeta}u\right) + \left(\frac{\partial}{\partial s}w\right),
\end{aligned} \tag{2}$$

where $Z = 1/(s\sin(\gamma) + \zeta\cos(\gamma))$.

The stress-strain relation according to constitutive equations for isotropic material in matrix form is defined as follows:

$$\begin{bmatrix}\sigma_{ss}\\ \sigma_{\theta\theta}\\ \sigma_{\zeta\zeta}\\ \tau_{\theta\zeta}\\ \tau_{s\zeta}\\ \tau_{s\theta}\end{bmatrix} = \begin{bmatrix} Q_{11} & Q_{12} & Q_{13} & 0 & 0 & 0\\ Q_{21} & Q_{22} & Q_{23} & 0 & 0 & 0\\ Q_{31} & Q_{32} & Q_{33} & 0 & 0 & 0\\ 0 & 0 & 0 & Q_{44} & 0 & 0\\ 0 & 0 & 0 & 0 & Q_{55} & 0\\ 0 & 0 & 0 & 0 & 0 & Q_{66}\end{bmatrix} \begin{bmatrix}\varepsilon_{ss} - \alpha(\zeta)\,T(\zeta)\\ \varepsilon_{\theta\theta} - \alpha(\zeta)\,T(\zeta)\\ \varepsilon_{\zeta\zeta} - \alpha(\zeta)\,T(\zeta)\\ \varepsilon_{\theta\zeta}\\ \varepsilon_{s\zeta}\\ \varepsilon_{s\theta}\end{bmatrix}, \tag{3}$$

where σ_{ij} and τ_{ij} indicate the normal and shear stress components, respectively, and ε_{ij} denotes the strain components, $T(\zeta)$ represents the temperature distribution through thickness obtained from the steady-state heat conduction equation, and also $\alpha(\zeta)$ is the coefficient of thermal expansion. The elastic coefficients for isotropic materials in terms of elastic stiffness and Poisson's ratio are expressed as follows:

$$\begin{aligned}
\lambda &= \frac{\upsilon E}{(1+\upsilon)(1-2\upsilon)},\\
G &= \frac{E}{2(1+\upsilon)},\\
Q_{11} &= \lambda + 2G,\\
Q_{12} &= \lambda,\\
Q_{44} &= G,\\
Q_{12} &= Q_{21} = Q_{13} = Q_{31} = Q_{32} = Q_{23},\\
Q_{11} &= Q_{22} = Q_{33},\\
Q_{44} &= Q_{55} = Q_{66}.
\end{aligned} \tag{4}$$

Assuming quasistatic state, the acceleration terms can be eliminated from the equilibrium equations [26]. With this assumption, the equilibrium equations in s, θ, and ζ directions in the presence of body force are given in (5a)–(5c), respectively, as

$$\begin{aligned}
&\frac{\partial\sigma_{ss}}{\partial s} + \frac{\partial\tau_{s\zeta}}{\partial\zeta}\\
&\quad + Z\left((\sigma_{ss} - \sigma_{\theta\theta})\sin(\gamma) + \left(\tau_{s\zeta} + \frac{\partial\tau_{s\theta}}{\partial\theta}\right)\cos(\gamma)\right)\\
&\quad + f_{\text{Cb-}s} = 0,
\end{aligned} \tag{5a}$$

$$\begin{aligned}
&\frac{\partial\tau_{s\theta}}{\partial s} + \frac{\partial\tau_{\zeta\theta}}{\partial\zeta}\\
&\quad + Z\left(\left(\frac{\partial\sigma_{\theta\theta}}{\partial\theta}\right) + 2\tau_{\zeta\theta}\cos(\gamma) + 2\tau_{s\theta}\sin(\gamma)\right)\\
&\quad + f_{\text{Cb-}\theta} = 0,
\end{aligned} \tag{5b}$$

$$\begin{aligned}
&\frac{\partial\tau_{s\zeta}}{\partial s} + \frac{\partial\sigma_{\zeta\zeta}}{\partial\zeta}\\
&\quad + Z\left(\left(\frac{\partial\tau_{\zeta\theta}}{\partial\theta}\right) + \tau_{s\zeta}\sin(\gamma) + (\sigma_{\zeta\zeta} - \sigma_{\theta\theta})\cos(\gamma)\right)\\
&\quad + f_{\text{Cb-}\zeta} = 0.
\end{aligned} \tag{5c}$$

Centrifugal body force components in designated conical coordinate knowing that the cone radius at any point along its generator is $R(s) = \cos(\gamma)\zeta + \sin(\gamma)s$ are calculated by the following formulations:

$$\begin{aligned}
f_{\text{Cb}} &= \rho R(s)\,\omega^2;\\
f_{\text{Cb-}s} &= \rho_0\left(1 + \frac{\zeta}{h_{\text{sh}}}\right)^n(\cos(\gamma)\zeta + \sin(\gamma)s)\,\omega^2\sin(\gamma);\\
f_{\text{Cb-}\theta} &= 0;\\
f_{\text{Cb-}\zeta} &= \rho_0\left(1 + \frac{\zeta}{h_{\text{sh}}}\right)^n(\cos(\gamma)\zeta + \sin(\gamma)s)\,\omega^2\cos(\gamma).
\end{aligned} \tag{6}$$

Using (2), (3), and (6) and substituting them into (5a)–(5c), the following equilibrium equations in terms of displacement components and temperature in the three

directions of s, θ, and ζ are derived in (7a)–(7c), respectively, as follows:

$$\begin{aligned}
&\frac{E_0\left(1+\zeta/h_{\mathrm{sh}}\right)^n}{(1+\upsilon)(1-2\upsilon)}\left((1-\upsilon)\left(\frac{\partial^2 u}{\partial s^2}\right)+\upsilon\left(\frac{\partial^2 w}{\partial s\partial\zeta}\right.\right.\\
&\quad+Z^2\left(\frac{\partial v}{\partial\theta}\sin(\gamma)+u\sin^2(\gamma)+w\sin(\gamma)\cos(\gamma)\right.\\
&\quad-2\left(\frac{\partial v}{\partial\theta}+u\sin(\gamma)+w\cos(\gamma)\right)\sin(\gamma)\Big)\\
&\quad\left.\left.+Z\left(\frac{\partial^2 v}{\partial\theta\partial s}+\frac{\partial u}{\partial s}\sin(\gamma)+\frac{\partial w}{\partial s}\cos(\gamma)\right)\right)\right)\\
&+\frac{E_0\left(1+\zeta/h_{\mathrm{sh}}\right)^n}{2(1+\upsilon)}\left(\frac{\partial^2 u}{\partial\zeta^2}+\frac{\partial^2 w}{\partial s\partial\zeta}\right.\\
&\quad+\frac{n\left(\partial u/\partial\zeta+\partial w/\partial s\right)}{\left(1+\zeta/h_{\mathrm{sh}}\right)}+Z\left(2\left(\frac{\partial u}{\partial s}\right.\right.\\
&\quad\left.-Z\left(\frac{\partial v}{\partial\theta}+u\sin(\gamma)+w\cos(\gamma)\right)\right)\sin(\gamma)+\left(\frac{\partial u}{\partial\zeta}\right.\\
&\quad+\frac{\partial w}{\partial s}+\frac{\partial^2 v}{\partial\theta\partial s}+Z\left(\frac{\partial^2 u}{\partial\theta^2}-\frac{\partial v}{\partial\theta}\sin(\gamma)\right)\Big)\\
&\quad\left.\left.\cdot\cos(\gamma)\right)\right)+\rho_0\left(1+\frac{\zeta}{h_{\mathrm{sh}}}\right)^n(\cos(\gamma)\zeta+\sin(\gamma)s)\\
&\quad\cdot\omega^2\sin(\gamma)=0,
\end{aligned}\tag{7a}$$

$$\begin{aligned}
&\frac{E_0\left(1+\zeta/h_{\mathrm{sh}}\right)^n}{2(1+\upsilon)}\left(\frac{\partial^2 v}{\partial s^2}+\frac{\partial^2 v}{\partial\zeta^2}\right.\\
&\quad+\frac{n\left(Z\left(\partial w/\partial\theta-v\cos(\gamma)\right)+\partial v/\partial\zeta\right)}{h_{\mathrm{sh}}\left(1+\zeta/h_{\mathrm{sh}}\right)}\\
&\quad+Z^2\left(\left(v\sin(\gamma)-\frac{\partial u}{\partial\theta}\right)\sin(\gamma)+\left(v\cos(\gamma)\right.\right.\\
&\quad\left.-\frac{\partial w}{\partial\theta}\right)\cos(\gamma)\Big)+Z\left(\frac{\partial^2 u}{\partial\theta\partial s}-\frac{\partial v}{\partial s}\sin(\gamma)+\frac{\partial^2 w}{\partial\theta\partial\zeta}\right.\\
&\quad\left.\left.-\frac{\partial v}{\partial\zeta}\cos(\gamma)\right)\right)+\frac{ZE_0\left(1+\zeta/h_{\mathrm{sh}}\right)^n}{(1+\upsilon)(1-2\upsilon)}\left((1-\upsilon)\right.\\
&\quad\cdot\left(Z\left(\frac{\partial^2 v}{\partial\theta^2}+\frac{\partial u}{\partial\theta}\sin(\gamma)+\frac{\partial w}{\partial\theta}\cos(\gamma)\right)\right)\\
&\quad+\upsilon\left(\frac{\partial^2 u}{\partial\theta\partial s}+\frac{\partial^2 w}{\partial\theta\partial\zeta}\right)+(1-2\upsilon)\left(\left(\frac{\partial v}{\partial\zeta}\right.\right.\\
&\quad+Z\left(\frac{\partial w}{\partial\theta}-v\cos(\gamma)\right)\Big)\cos(\gamma)+\left(\frac{\partial v}{\partial s}\right.\\
&\quad\left.\left.\left.+Z\left(\frac{\partial u}{\partial\theta}-v\sin(\gamma)\right)\right)\sin(\gamma)\right)\right)=0,
\end{aligned}\tag{7b}$$

$$\begin{aligned}
&\frac{E_0\left(1+\zeta/h_{\mathrm{sh}}\right)^n}{2(1+\upsilon)}\left(\frac{\partial^2 u}{\partial s\partial\zeta}+\frac{\partial^2 w}{\partial s^2}\right)\\
&+\frac{E_0\left(1+\zeta/h_{\mathrm{sh}}\right)^n n}{h_{\mathrm{sh}}\left(1+\zeta/h_{\mathrm{sh}}\right)(1+\upsilon)(1-2\upsilon)}\left((1-\upsilon)\left(\frac{\partial w}{\partial\zeta}\right)\right.\\
&+\upsilon\left(\frac{\partial u}{\partial s}+Z\left(\frac{\partial v}{\partial\theta}+u\sin(\gamma)+w\cos(\gamma)\right)\right)-(1\\
&+\upsilon)\alpha\left(1+\frac{\zeta}{h_{\mathrm{sh}}}\right)^n T\Big)+\frac{E_0\left(1+\zeta/h_{\mathrm{sh}}\right)^n}{(1+\upsilon)(1-2\upsilon)}\left((1-\upsilon)\right.\\
&\cdot\left(\frac{\partial^2 w}{\partial\zeta^2}\right)+\upsilon\left(\frac{\partial^2 u}{\partial s\partial\zeta}+Z^2\left(\frac{\partial v}{\partial\theta}\cos(\gamma)\right.\right.\\
&+u\sin(\gamma)\cos(\gamma)+w\cos^2(\gamma)\\
&-2\left(\frac{\partial v}{\partial\theta}+u\sin(\gamma)+w\cos(\gamma)\right)\cos(\gamma)\Big)\\
&\left.+Z\left(\frac{\partial^2 v}{\partial\theta\partial\zeta}+\frac{\partial u}{\partial\zeta}\sin(\gamma)+\frac{\partial w}{\partial\zeta}\cos(\gamma)\right)\right)-(1\\
&+\upsilon)\left(\frac{\alpha E_0\left(1+\zeta/h_{\mathrm{sh}}\right)^n m_3 T(\zeta)}{h_{\mathrm{sh}}\left(1+\zeta/h_{\mathrm{sh}}\right)}+\alpha\left(1\right.\right.\\
&\left.\left.+\frac{\zeta}{h_{\mathrm{sh}}}\right)^n\frac{\partial T}{\partial\zeta}\right)\Big)+\frac{ZE_0\left(1+\zeta/h_{\mathrm{sh}}\right)^n}{2(1+\upsilon)}\left(\frac{\partial^2 v}{\partial\theta\partial\zeta}\right.\\
&+\left(\frac{\partial u}{\partial\zeta}+\frac{\partial w}{\partial s}\right)\sin(\gamma)+Z\left(\frac{\partial^2 w}{\partial\theta^2}-\frac{\partial v}{\partial\theta}\cos(\gamma)\right)\\
&+2\left(\frac{\partial w}{\partial\zeta}-Z\left(\frac{\partial v}{\partial\theta}+u\sin(\gamma)+w\cos(\gamma)\right)\right)\\
&\left.\cdot\cos(\gamma)\right)+\rho_0\left(1+\frac{\zeta}{h_{\mathrm{sh}}}\right)^n(\cos(\gamma)\zeta+\sin(\gamma)s)\\
&\cdot\omega^2\cos(\gamma)=0.
\end{aligned}\tag{7c}$$

The steady-state heat conduction equation without heat generation in the conical coordinate can be written as

$$\begin{aligned}
&\left(\frac{K(\zeta)\cos(\gamma)}{(R_1+s\sin(\gamma)+\zeta\cos(\gamma))}\right)\frac{\partial}{\partial\zeta}T(\zeta)\\
&\quad+K(\zeta)\frac{\partial^2}{\partial\zeta^2}T(\zeta)+\frac{\partial}{\partial\zeta}K(\zeta)\frac{\partial}{\partial\zeta}T(\zeta)=0.
\end{aligned}\tag{8}$$

The mathematical expressions of mechanical and thermal boundary conditions for the two considered cases including clamped and simply supported at top and bottom of truncated conical shell are described as follows:

$$\begin{aligned}
s=\frac{R_1}{\sin(\gamma)}:\quad &u=0,\\
&w=0,
\end{aligned}$$

$$
\begin{aligned}
&v = 0,\\
&T_t = 0,\\
s = \frac{R_1}{\sin(\gamma)} + L:\quad &u = 0,\\
&w = 0,\\
&v = 0,\\
&T_b = 0
\end{aligned}
\tag{9a}
$$

$$
\begin{aligned}
s = \frac{R_1}{\sin(\gamma)}:\quad &\sigma_{ss} = 0,\\
&w = 0,\\
&v = 0,\\
&T_t = 0,\\
s = \frac{R_1}{\sin(\gamma)} + L:\quad &\sigma_{ss} = 0,\\
&w = 0,\\
&v = 0,\\
&T_b = 0.
\end{aligned}
\tag{9b}
$$

For both axisymmetric and asymmetric cases, the inner surface of conical shell is kept at zero and the outer surface is varied at constant temperature T_{out}. Thus, the following mechanical and thermal boundary conditions must be satisfied for the inner and outer surfaces:

$$
\begin{aligned}
\zeta = 0:\quad &\sigma_{\zeta\zeta} = 0,\\
&\tau_{s\zeta} = 0,\\
&\tau_{\theta\zeta} = 0,\\
&T_{\text{in}} = 0,\\
\zeta = h_{\text{sh}}:\quad &\sigma_{\zeta\zeta} = 0,\\
&\tau_{s\zeta} = 0,\\
&\tau_{\theta\zeta} = 0,\\
&T_O = T_o.
\end{aligned}
\tag{10}
$$

3. The Method of Solution

The DQ method as powerful discretization tool is applied to transform a system of resulting differential equations to a system of algebraic equations. The general rule of DQM postulates that derivative of any continuous function $f(s,\theta,\zeta)$ with respect to space variable at any discrete point in the domain can be expressed as a linear weighted linear summation of all the functional values in the whole domain as follows [27]:

$$
\begin{aligned}
\left.\frac{\partial f}{\partial \zeta}\right|_{ijk} &\approx \sum_{l=1}^{N} A_{il} f_{ljk},\\
\left.\frac{\partial f}{\partial \theta}\right|_{ijk} &\approx \sum_{m=1}^{M} B_{jm} f_{imk},\\
\left.\frac{\partial f}{\partial s}\right|_{ijk} &\approx \sum_{n=1}^{P} C_{kn} f_{ijn},\\
\left.\frac{\partial^2 f}{\partial \zeta^2}\right|_{ijk} &\approx \sum_{l=1}^{N} A^{(2)}{}_{il} f_{ljk},\\
\left.\frac{\partial^2 f}{\partial \theta^2}\right|_{ijk} &\approx \sum_{m=1}^{M} B^{(2)}{}_{jm} f_{imk},\\
\left.\frac{\partial^2 f}{\partial s^2}\right|_{ijk} &\approx \sum_{n=1}^{P} C^{(2)}{}_{kn} f_{ijn},\\
\left.\frac{\partial^2 f}{\partial \theta \partial \zeta}\right|_{ijk} &\approx \sum_{l=1}^{N}\sum_{m=1}^{M} A^{(1)}{}_{il} B^{(1)}{}_{jm} f_{lmk},\\
\left.\frac{\partial^2 f}{\partial s \partial \zeta}\right|_{ijk} &\approx \sum_{l=1}^{N}\sum_{n=1}^{P} A^{(1)}{}_{il} C^{(1)}{}_{kn} f_{ljn},\\
\left.\frac{\partial^2 f}{\partial \theta \partial s}\right|_{ijk} &\approx \sum_{m=1}^{M}\sum_{n=1}^{P} B^{(1)}{}_{jm} C^{(1)}{}_{kn} f_{imn},
\end{aligned}
\tag{11}
$$

where A^m, B^m, and C^m denote the weighting coefficients for the mth-order derivatives of the function $f(s,\theta,\zeta)$ in thickness direction at mesh point ζ_i, along the generator at mesh point s_i and circumferential direction at mesh point θ_i, respectively. Furthermore, P, M, and N are the numbers of sampling points along the s, θ, and ζ, respectively. In this study, polynomial differential quadrature (PDQ) is employed to determine the weighting coefficients along ζ and s directions and the Fourier expansion-based differential quadrature (FDQ) is used to compute the weighting coefficient along the circumferential direction. The weighting coefficients are calculated according to following explicit formulations [27]:

$$
\begin{aligned}
A^{(1)}_{i,j} &= \left(\frac{1}{x_j - x_i}\right) \prod_{\substack{k=1\\ k\neq i,j}}^{N} \frac{x_i - x_k}{x_j - x_k}, \quad i \neq j,\\
A^{(1)}_{i,i} &= \sum_{\substack{k=1\\ k\neq i}}^{N} \frac{1}{x_i - x_k},\\
A^{(2)}_{i,j} &= \sum_{k=1}^{N} A^{(1)}_{i,k} A^{(1)}_{k,j},
\end{aligned}
\tag{12a}
$$

$$\eta_{ij} = \frac{q(x_i)}{2\sin\left(\left(x_i - x_j\right)/2\right)\left(\prod_{k=0}^{M}\sin\left(\left(x_j - x_k\right)/2\right)\right)}, \quad i \neq j,$$

$$\eta_{ii} = -\sum_{\substack{j=0 \\ i\neq j}}^{M}\eta_{ij},$$

$$C^{(1)}{}_{ij} = \eta_{ij}\left(2\eta_{ii} - \cot\left(\frac{x_i - x_j}{2}\right)\right), \quad i \neq j \tag{12b}$$

$$C^{(1)}{}_{ii} = -\sum_{\substack{j=0 \\ i\neq j}}^{M} C^{(1)}{}_{ij},$$

$$C^{(2)}_{i,j} = \sum_{j=0}^{M} C^{(1)}_{j,m} C^{(1)}_{m,j}.$$

Using (11) and applying relations in (12a) and (12b), the DQ analogs of the governing, related boundary conditions, and heat transfer equations are achieved. The discretized forms of equations using DQ technique are given in detail in Appendix. The system of algebraic equations discretized by DQM is effectively solved based on the semismooth Newton-Raphson iteration procedure as follows. Consider the vector of unknown variables $\vec{g}$ and the resulting governing and boundary equations q_i:

$$gg1_{P\times M\times N} = \begin{Bmatrix} u_{1,1,1} \\ \cdot \\ \cdot \\ \cdot \\ u_{N,M,P} \end{Bmatrix},$$

$$gg2_{P\times M\times N} = \begin{Bmatrix} v_{1,1,1} \\ \cdot \\ \cdot \\ v_{N,M,P} \end{Bmatrix},$$

$$gg3_{P\times M\times N} = \begin{Bmatrix} w_{1,1,1} \\ \cdot \\ \cdot \\ w_{N,M,P} \end{Bmatrix}, \tag{13a}$$

$$gg4_{N} = \begin{Bmatrix} T_{1,1,1} \\ \cdot \\ T_{1,1,N} \end{Bmatrix},$$

$$\vec{g} = \begin{Bmatrix} gg1 \\ gg2 \\ gg3 \\ gg4 \end{Bmatrix},$$

$$q_i = \begin{Bmatrix} q_1 \\ \cdot \\ \cdot \\ q_{(4P\times M\times N+N)} \end{Bmatrix} = 0. \tag{13b}$$

The system of equation $q_i = 0$ with unknown variable vector $\vec{g}$ can be solved using the following Newton-Raphson iteration scheme:

$$g^{k+1} = g^k - \left(\frac{q^k}{(\partial q/\partial g)^k}\right), \tag{14}$$

where the applied notation kth in the definition of Newton technique is iteration number. It should be noted that the solution starts from $g^1 = 0$. In (14), g^{k+1} is successively replaced by previous iteration and this procedure continues until difference between two successive iterations equals designated tolerance or $|g^{k+1} - g^k| < 10^{-6}$.

4. Numerical Results and Discussion

The coordinates of the grid points are chosen based on the Chebyshev-Gauss-Lobatto relation as follows [27]:

In the s-direction,

$$s_i = L_1 + \frac{L}{2}\left(1 - \cos\left(\frac{i-1}{P-1}\pi\right)\right), \quad i = 1, \ldots, P. \tag{15}$$

In the θ-direction,

$$\theta_j = \frac{j-1}{M}2\pi, \quad j = 1, \ldots, M. \tag{16}$$

In the ζ –direction,

$$\zeta_i = \frac{h_{\text{sh}}}{2}\left(1 - \cos\left(\frac{i-1}{N-1}\pi\right)\right), \quad i = 1, \ldots, N. \tag{17}$$

The geometrical properties of truncated conical shell are considered to be $L = 1(\text{m})$, $\gamma = 15^0$, $h_{\text{sh}} = 0.2(\text{m})$, and $R_2 = 0.5(\text{m})$. The truncated conical shell is assumed to be made up of aluminum with the following material properties [28]:

$$\begin{aligned} E_0 &= 70\ \text{GPa}, \\ \nu &= 0.33, \\ \alpha_0 &= 24 \times 10^{-6}\ 1/^{\circ}\text{C}, \\ K_0 &= 92.6 \times 10^{-6}\ \text{W/m}^{\circ}\text{C}, \\ \rho &= 2700\ \text{kg/m}^3. \end{aligned} \tag{18}$$

Here, the presented results are based on the nondimensional forms of thickness displacement, temperature, and stresses as defined in the following:

$$\overline{\sigma}_{ij} = \frac{(1-\upsilon)\,\sigma_{ij}}{\left(4E_0\alpha_0 T + 2\rho_0\left(\cos(\gamma)\,\zeta + \sin(\gamma)\,s\right)^2\omega^2\right)},$$
$$\overline{w} = \frac{w}{h_{\mathrm{sh}}}, \tag{19}$$
$$\overline{T} = \frac{T}{T_o}.$$

In order to illustrate the convergence and accuracy of presented method, the thermoelastic problem of thick-walled FG spherical shell carried out by Eslami et al. [7] is chosen to validate the results obtained by the present approach. The problem considered was the thermoelastic analysis of 1D thick-walled FG spherical shell. Reference [7] assumed the material properties except Poisson's ratio to be varied along the thickness according to following power law rule:

$$E = E_0\,(r)^m,$$
$$\alpha = \alpha_0\,(r)^m, \tag{20}$$
$$K = K_0\,(r)^m,$$

where E_0, α_0, and K_0 are the modulus of elasticity, the coefficient of thermal expansion, and thermal conduction coefficient at inner radius, respectively, and m is the in-homogeneity constant. The inner and outer radii were assumed to be $a = 1\,(m)$ and $= 1.2\,(m)$, respectively. The used material properties were $E_0 = 200$ GPa and $\alpha_0 = 1.2 \times 10^{-6}\,1/^{\circ}\mathrm{C}$ and also the thermal and mechanical boundary conditions were supposed to be $T(a) = 10^{\circ}\mathrm{C}$, $T(b) = 0^{\circ}\mathrm{C}$, $\sigma_{rr}(a) = -50$ MPa, and $\sigma_{rr}(b) = 0$. Furthermore, for comparison, the values of circumferential stress and radial displacement for $m = 3$ are selected. Figure 2(a) shows the variations of nondimensional values of circumferential stress along radial direction computed by present method and [7]. It is observed from Figure 2(a) that the present numerical technique yields convergence at $N = 20$ and also the converged results are in an excellent agreement with those obtained by [7]. For more validation of the present approach, the variations of dimensionless radial displacement u/a along thickness calculated by DQM and with those achieved by [7] are demonstrated in Figure 2(b). According to Figure 2(b), for some values of $r/a = \overline{r}$, the dimensionless radial displacement u/a predicted by present approach is little higher than the values obtained by [7] and with other ranges of $\overline{r}$ is smaller. It can be concluded from Figure 2(b) that the good consistency (maximum discrepancy of 2.5%) between present numerical technique and [7] is depicted that confirms the efficiency and reliability of the present numerical method. For more assurance of the accuracy of present method, another pressure vessel component under thermomechanical loading modelled by [24] is performed in Figures 3(a) and 3(b).

A more convergence of the method is investigated by obtaining dimensionless radial displacement for the thermoelastic behavior of thick-walled FG cylindrical shell carried out by [24]. The same geometrical and material properties and also thermal and mechanical boundary conditions used in [7] were applied in [24]. Table 1 is based on the behavior of FG cylindrical shell at the inner wall. According to the presented results in Table 1, for dimensionless radial displacement u/a and for FG in-homogeneity constant $m = 1$, in (20), it is obvious that the converged results are achieved by $N = 20$. Moreover, for more certainty of applicability of the used numerical technique in the present paper, another comparison is performed for the thermoelastic analysis of thick-walled FG cylindrical shell carried out by [24]. As one can see from Figures 3(a) and 3(b), the excellent agreements and inconsiderable discrepancy exist between present approach and [24].

4.1. Axisymmetric Problem. In this section, numerical results for axisymmetric case of FG truncated conical shell are calculated at the midpoint $s = L_1 + L/2$ and graphically presented and discussed in Figures (4)–(6). Figures 4(a)–4(f) demonstrate the effects of in-homogeneity constant n, on the thickness distribution of the displacement component in thickness direction, stress components, and temperature field. FG truncated conical shell rotates with angular rotating speed $\omega = 500$ rad/s and is subjected to temperature gradient through thickness with the inner surface temperature of zero and the outer surface temperature of $T_o = 100^{\circ}\mathrm{C}$. It can be observed from Figure 4(a) that the values of normalized thickness stress $\overline{\sigma}_{\zeta\zeta}$ increase with changing of power law index n from 1 to 3. It is also found that the prescribed mechanical boundary conditions of the problem at the inner and outer surfaces are satisfied. Moreover, the position that $\overline{\sigma}_{\zeta\zeta}$ reaches the maximum value is closer to the outer surface at $\simeq 0.12\,(m)$. It can be also found from Figure 4(b) that changing power law index n from 1 to 3 causes increase of the values of dimensionless circumferential stress $\overline{\sigma}_{\theta\theta}$. It is interesting to note that the influences of n are more pronounced on the regions closer to outer surface than those closer to the inner surface. Note that $\overline{\sigma}_{\theta\theta}$ reaches maximum value at $\simeq 0.12\,(m)$.

Figure 4(c) illustrates that the absolute values of $\overline{\sigma}_{ss}$ increase as n varies from 1 to 3. It is seen from Figure 4(d) that the absolute values of normalized shear stress $\overline{\tau}_{s\zeta}$ with concave profile like $\overline{\sigma}_{\zeta\zeta}$ in Figure 4(a) increase by increasing n from 1 to 3. It is interesting to note that $\overline{\tau}_{s\zeta}$ achieves its maximum values at $\zeta \simeq 0.12$ (m). Moreover, from Figure 4(e) it is obvious that the amplitudes of dimensionless displacement $\overline{w}$ increase through thickness due to increasing of n. Temperature distribution along thickness for various n is plotted in Figure 4(f). It can be inferred that the absolute values of temperature monotonically enhance with increasing power law index n. The influences of temperature gradient through thickness on the thickness distributions of dimensionless stress component and thickness displacement are illustrated in Figures 5(a)–5(e). It is assumed that FG truncated conical shell rotates with rotating angular speed $\omega = 500$ rad/s and also T_o is held at zero and T_{in} is varied. As Figure 5(a) reveals, the amplitudes of dimensionless thickness stress $\overline{\sigma}_{\zeta\zeta}$ increase as temperature gradient through thickness is elevated and also thickness component of stress is tensile

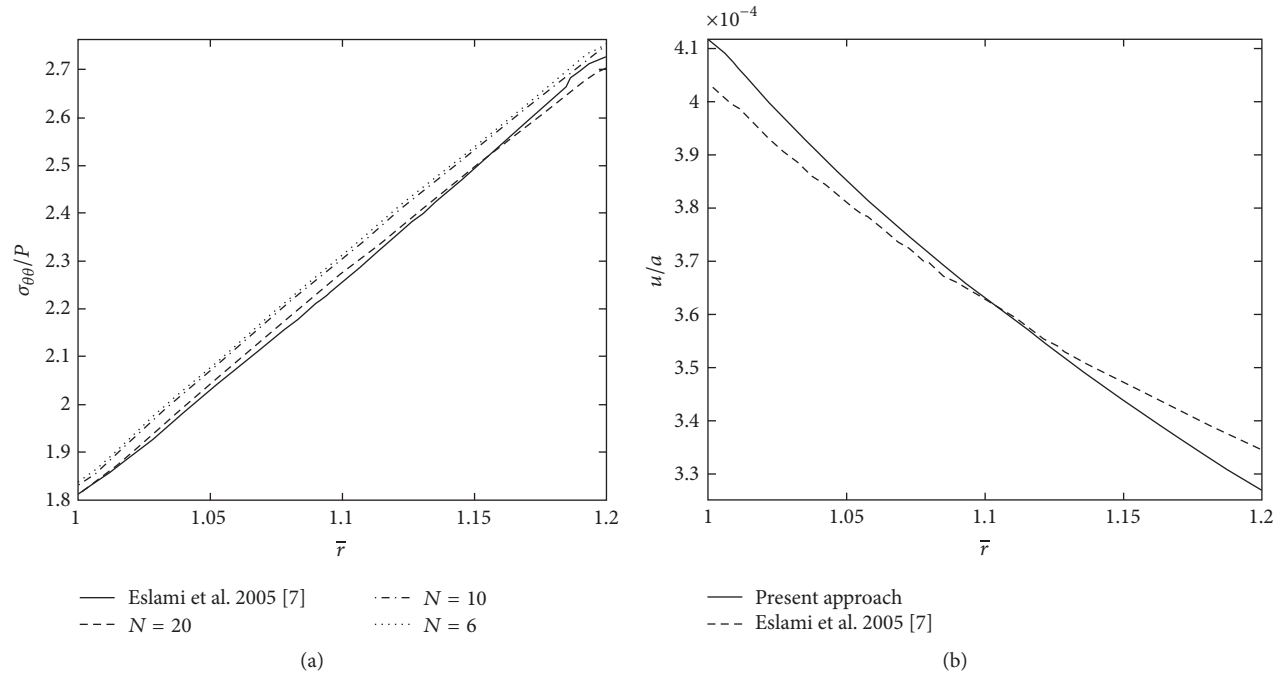

Figure 2: Comparisons of present approach and [7]. (a) Radial distribution of circumferential stress for an FGM spherical shell; (b) radial distribution of radial displacement for an FGM spherical shell.

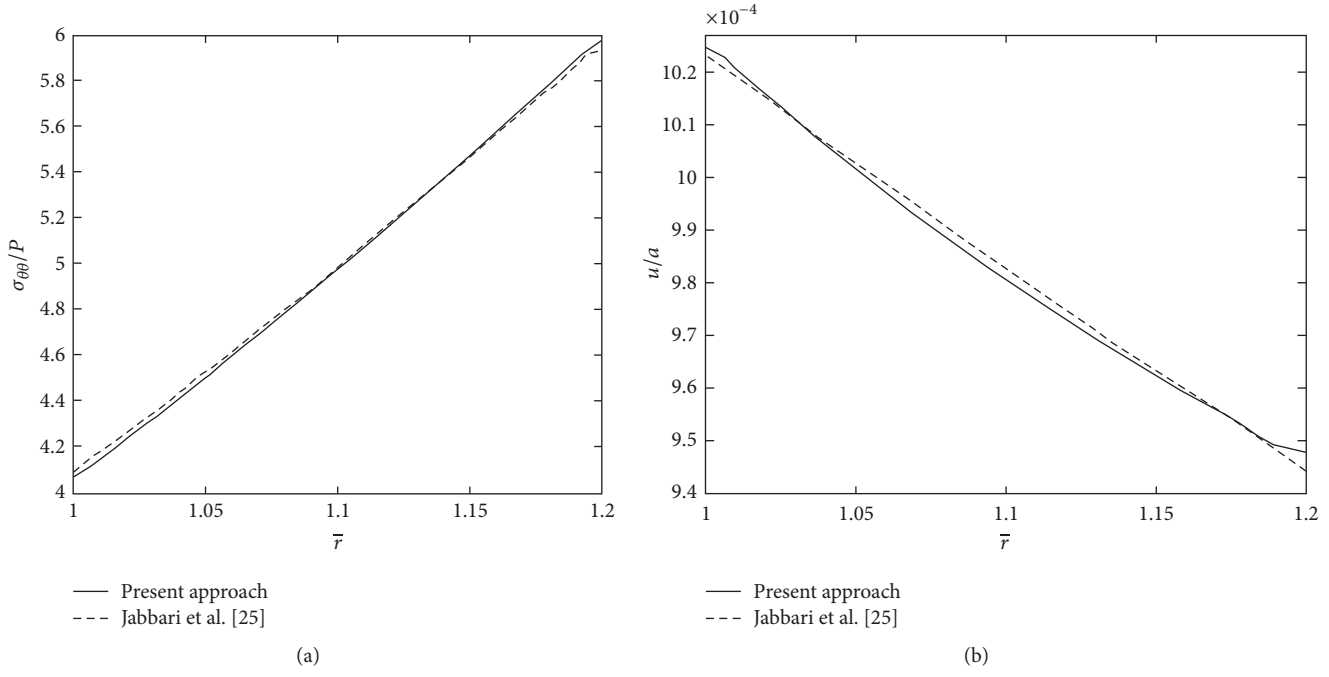

Figure 3: Comparisons of present approach and [24]. (a) Radial distribution of circumferential stress for an FGM cylindrical shell; (b) radial distribution of radial displacement for an FGM cylindrical shell.

Table 1: Convergence behavior of dimensionless radial displacement u/a for thermoelastic problem of FG cylindrical shell carried out by [24].

The number of grid points	$N = 6$ Present approach	$N = 10$ Present approach	$N = 20$ Present approach	Jabbari et al. [24]
u/a	0.00119	0.0011225	0.00124	0.00124

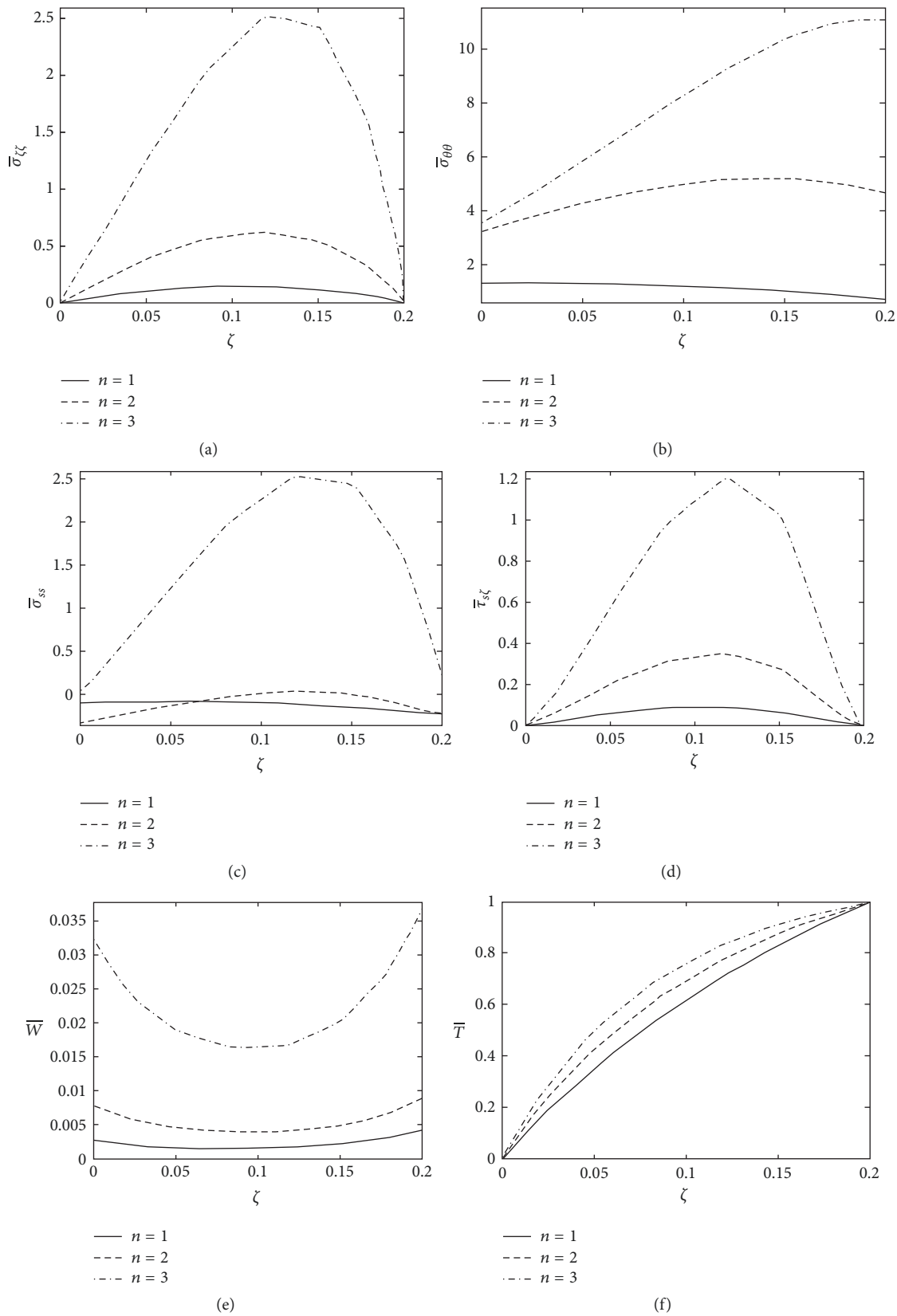

Figure 4: (a) The influence of power law index n on the stress component in ζ through thickness distribution. (b) The influence of power law index n on the stress component in θ direction through thickness distribution. (c) The influence of power law index n on the stress component in s direction through thickness distribution. (d) The influence of power law index n on the shear stress through thickness distribution. (e) The influence of power law index n on displacement component in ζ direction through thickness distribution. (f) The influence of power law index n on the temperature through thickness distribution.

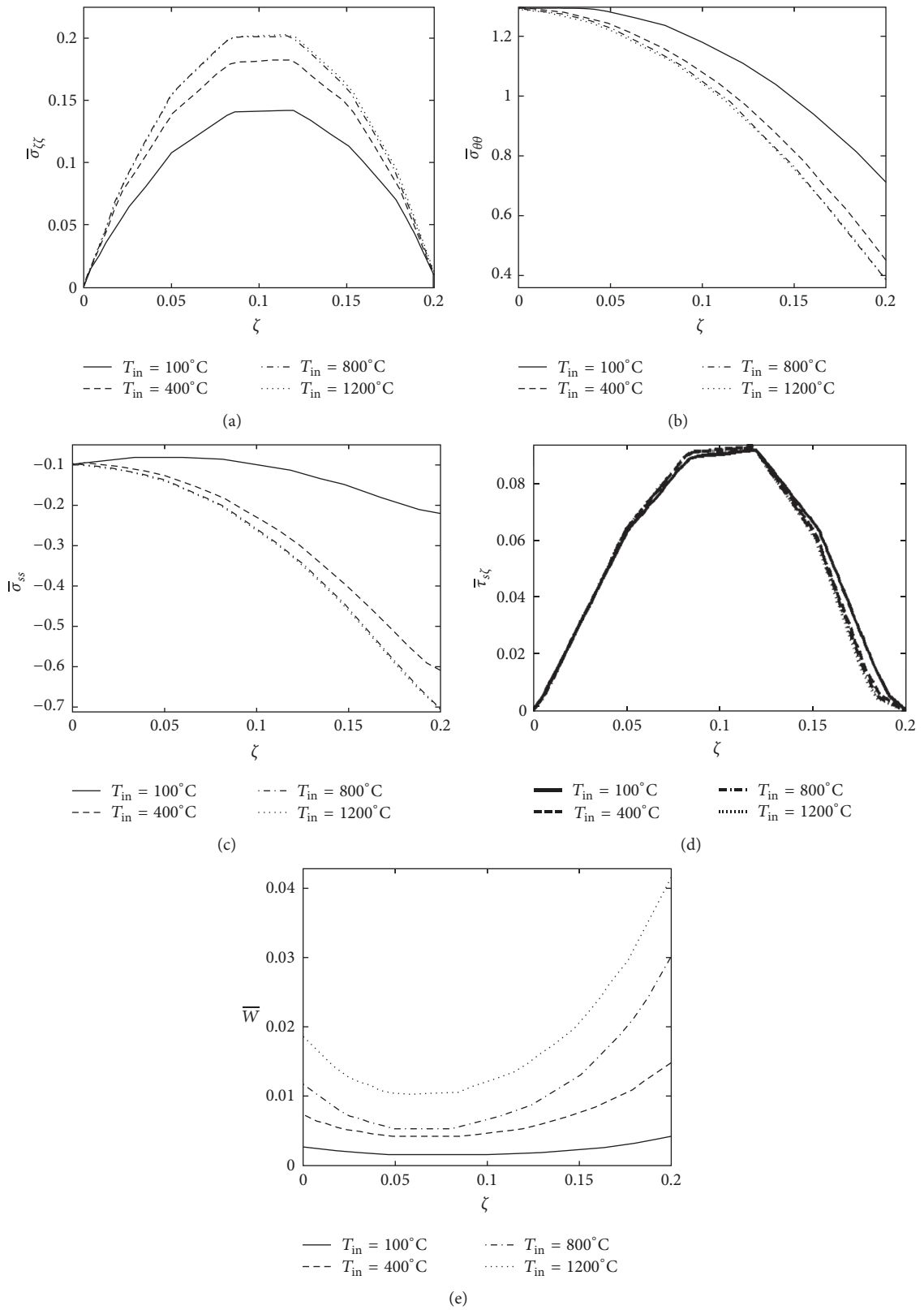

Figure 5: (a) The influence of thermal load on the stress component in ζ direction through thickness distribution. (b) The influence of thermal load on the stress component in θ direction through thickness distribution. (c) The influence of thermal load on the stress component in s direction through thickness distribution. (d) The influence of thermal load on the shear stress through thickness distribution. (e) The influence of thermal load on the displacement component in ζ direction, through thickness distribution.

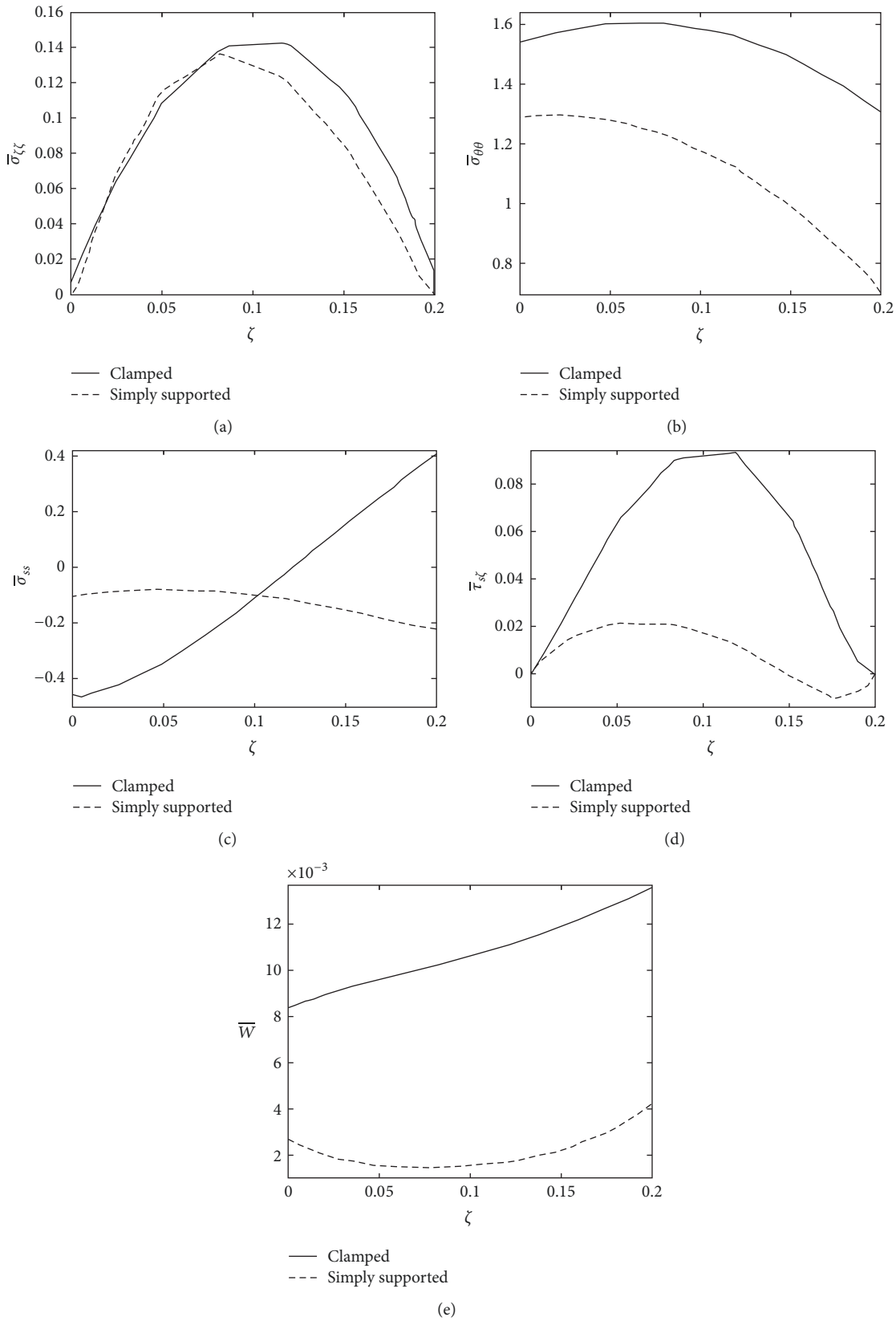

Figure 6: (a) The influence of boundary conditions on the stress component in ζ through thickness distribution. (b) The influence of boundary conditions on stress component in θ through thickness distribution. (c) The influence of boundary conditions on stress component in s direction through thickness distribution. (e) The influence of boundary conditions on the shear stress, through thickness distribution. (f) The influence of boundary conditions on displacement component in ζ direction, through thickness distribution.

throughout the thickness. It is observed in Figure 5(b) that as temperature gradient through thickness rises, the absolute values of the circumferential stress increase that these increases are more obvious for the regions closer to the outer periphery of FG tube. It must be mentioned that maximum value of $\overline{\sigma}_{\theta\theta}$ occurs at the inner wall. In Figure 5(c) same trend of Figure 4(b) is observed for the stress component in generator direction which means enhancing temperature gradient through thickness augments the compressive stresses. It is readily seen from Figure 5(d) that normalized shear stress $\overline{\tau}_{s\zeta}$ is slightly affected by thermal load which can be neglected. It can be inferred from Figures 5(c) and 5(d) that the maximum value of $\overline{\tau}_{s\zeta}$ occurs at middle of the thickness, whereas $\overline{\sigma}_{ss}$ attains maximum value at the outer wall of the thickness. Figure 5(e) reveals that the greater the temperature gradient through thickness is, the greater the displacement is obtained.

Figures 6(a)–6(e) illustrate the individual effects of two mechanical boundary conditions including clamped and simply supported on the parameters discussed in Figures 5(a)–5(e). In this section, FG truncated conical shell rotates at the constant rotating angular speed $\omega = 500\,\text{rad/s}$ and the values of temperature at the inner and outer surfaces of the shell are $T_{\text{in}} = 0^{\circ}\text{C}$ and $T_o = 100^{\circ}\text{C}$, respectively. It is viewed from Figure 6(a) that the effects of two boundary conditions on dimensionless stress component in thickness direction are small in the regions closer to the inner surface, whereas will be more pronounced in the regions closer to the outer surface. It is noteworthy to mention that the maximum value is shifted to the position closer to the outer surface. Figure 6(b) shows that the boundary conditions of clamped create higher values of circumferential stress than those of simply supported. It can be noted that the maximum value of $\overline{\sigma}_{\theta\theta}$ for both mechanical boundary conditions occurs at the inner wall of the shell. The effects of two prescribed edge boundary conditions on thickness variation of $\overline{\sigma}_{ss}$ are presented in Figure 6(c). It can be inferred from Figure 6(c) that changing boundary conditions from clamped to simply supported reduces the absolute values of dimensionless stress $\overline{\sigma}_{ss}$.

It should be noted that both boundary conditions under consideration in this paper exhibit symmetric response with respect to middle of the thickness. According to Figures 6(d) and 6(e), changing the boundary conditions from clamped to simply supported causes sharp reduction in the amplitudes of dimensionless shear stress $\overline{\tau}_{s\zeta}$ and thickness displacement $\overline{w}$.

4.2. Asymmetric Problem. For the asymmetric analysis, it is assumed that the FG truncated conical shell is under cosine type of internal pressure; that is, $P_{\text{in}} = P_0 \cos(\theta), P_0 = -50\,\text{MPa}$. In this section, the effects of the different angular velocity of ω, temperature gradient through thickness, and also the thickness of the shell on the stress components and thickness displacement for the three-dimensional problem of FG truncated conical shell are illustrated in Figures 7, 8, and 9, respectively. It must be noted that, in this section, geometrical parameters are given as in the previous section and all the circumferential variations of stress components and thickness displacement are calculated at location of $s = L_1 + L/2$ and $\zeta = h_{\text{sh}}/2$.

Figures 7(a)–7(e) demonstrate the distributions of dimensionless stress components and thickness displacement through circumferential direction with various rotating angular speed ω. Thermal boundary conditions for the inner and outer surfaces are assumed to be $T_{\text{in}} = 0^{\circ}\text{C}$ and $T_o = 100^{\circ}\text{C}$, respectively. From the plotted results, it can be well understood that as the angular velocity ω is augmented and centrifugal force is enhanced, the magnitudes of stress components become intensified, while increasing dimensionless shear stress $\overline{\tau}_{s\zeta}$ is almost negligible and can be disregarded. Figures 8(a)–8(e) reflect the sensitivities of dimensionless stress components and thickness displacement to temperature gradient through thickness. The rotating angular speed is assumed to be $\omega = 500\,\text{rad/s}$ and the temperature of inner surface is kept at zero and also the outer surface is varied. As noticed in Figures 8(a)–8(e), increasing the temperature gradient through thickness causes increase of the absolute values of normalized thickness stress and thickness displacement along the circumferential direction, whereas it causes reduction in the absolute values of circumferential stress and stress component along the generator. Moreover, we can observe that thermal loading negligibly affects the dimensionless shear stress $\overline{\tau}_{s\zeta}$ and can be disregarded.

In Figures 9(a)–9(e), circumferential distributions of the normalized stress components and thickness displacement are computed for different values of the shell thickness with conditions of $\omega = 500\,\text{rad/s}$, $T_{\text{in}} = 0^{\circ}\text{C}$, and $T_o = 100^{\circ}\text{C}$. It is obvious from Figures 8(a)–8(e) that as the shell becomes thicker, the values of the stress components and displacement are reduced. It is also seen that the discrepancy of dimensionless shear stress $\overline{\tau}_{s\zeta}$ for $h_{\text{sh}} = 0.2$, 0.3, and 0.4 (m) is negligible. In addition, the shear stress varies in parabolic manner for $h_{\text{sh}} = 0.2$, 0,3 and 0.4 (m), while it is distributed almost constant along the circumferential direction when h_{sh} equals 0.5 (m).

5. Conclusion

In this research, the thermoelastic behavior of FG rotating truncated conical shell under the individual effects of rotating angular speed, thermal loading, mechanical edge boundary conditions, and shell thickness were investigated. The material properties of FG were assumed to be graded in the thickness according to designated power law distribution, while Poisson's ratio was considered to be constant. Two versions of DQM including PDQ and FDQ were utilized to discretize and convert the resulting differential equations to the algebraic equations and then Newton-Raphson iteratively computed the numerical results. High rate of convergence and accuracy of the presented computational procedure were confirmed by comparing with those achieved by available literature. Some important conclusions based on the obtained results can be inferred as follows:

(A) Axisymmetric loading and boundary conditions:

(1) The absolute values of dimensionless stress components, thickness displacement, and temperature significantly increased as in-homogeneity

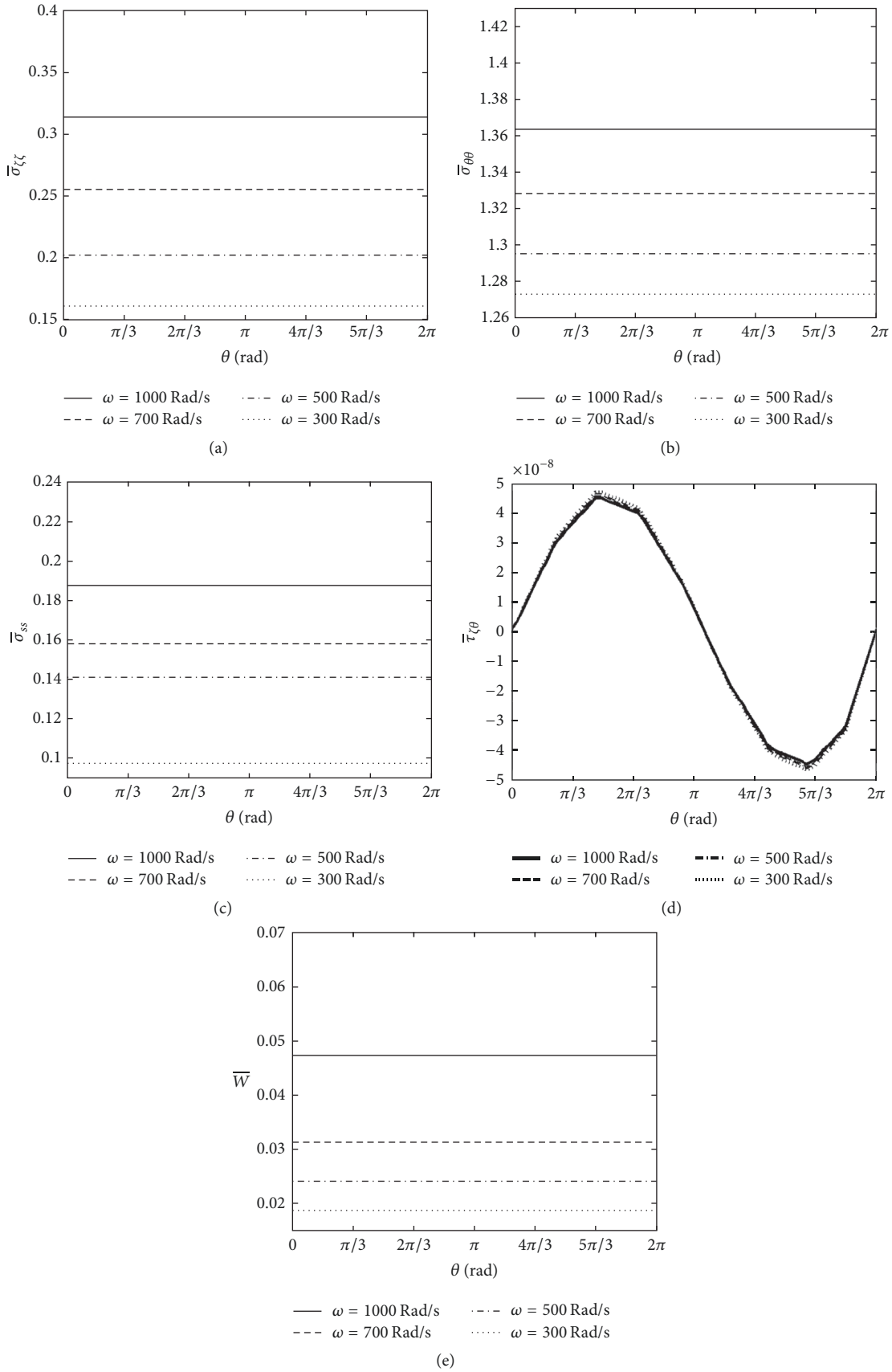

Figure 7: (a) The influence of rotating angular speed ω on the stress component in ζ direction through circumferential distribution. (b) The influence of rotating angular speed ω on the stress component in θ through circumferential distribution. (c) The influence of rotating angular speed ω on the stress component in s direction through circumferential distribution. (d) The influence of rotating angular speed ω on the shear stress through circumferential distribution. (e) The influence of rotating angular speed ω on the displacement component in ζ direction, through circumferential distribution.

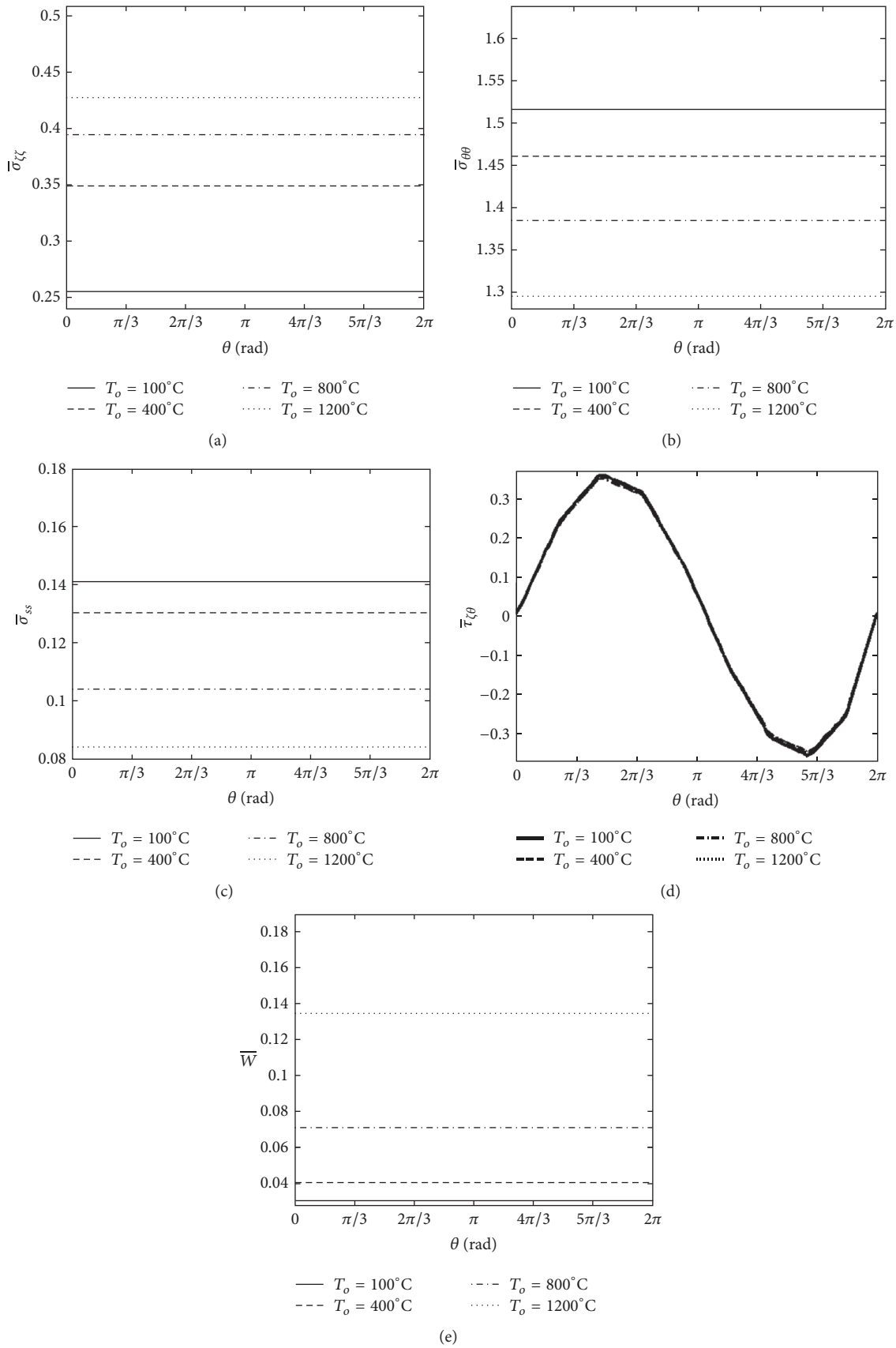

FIGURE 8: (a) The influence of thermal load on the stress component in ζ direction through circumferential distribution. (b) The influence of thermal load on the stress component in θ direction through circumferential distribution. (c) The influence of thermal load on the stress component in s direction through circumferential distribution. (d) The influence of thermal load on the shear stress through circumferential distribution. (e) The influence of thermal load on the displacement component in ζ direction, through circumferential distribution.

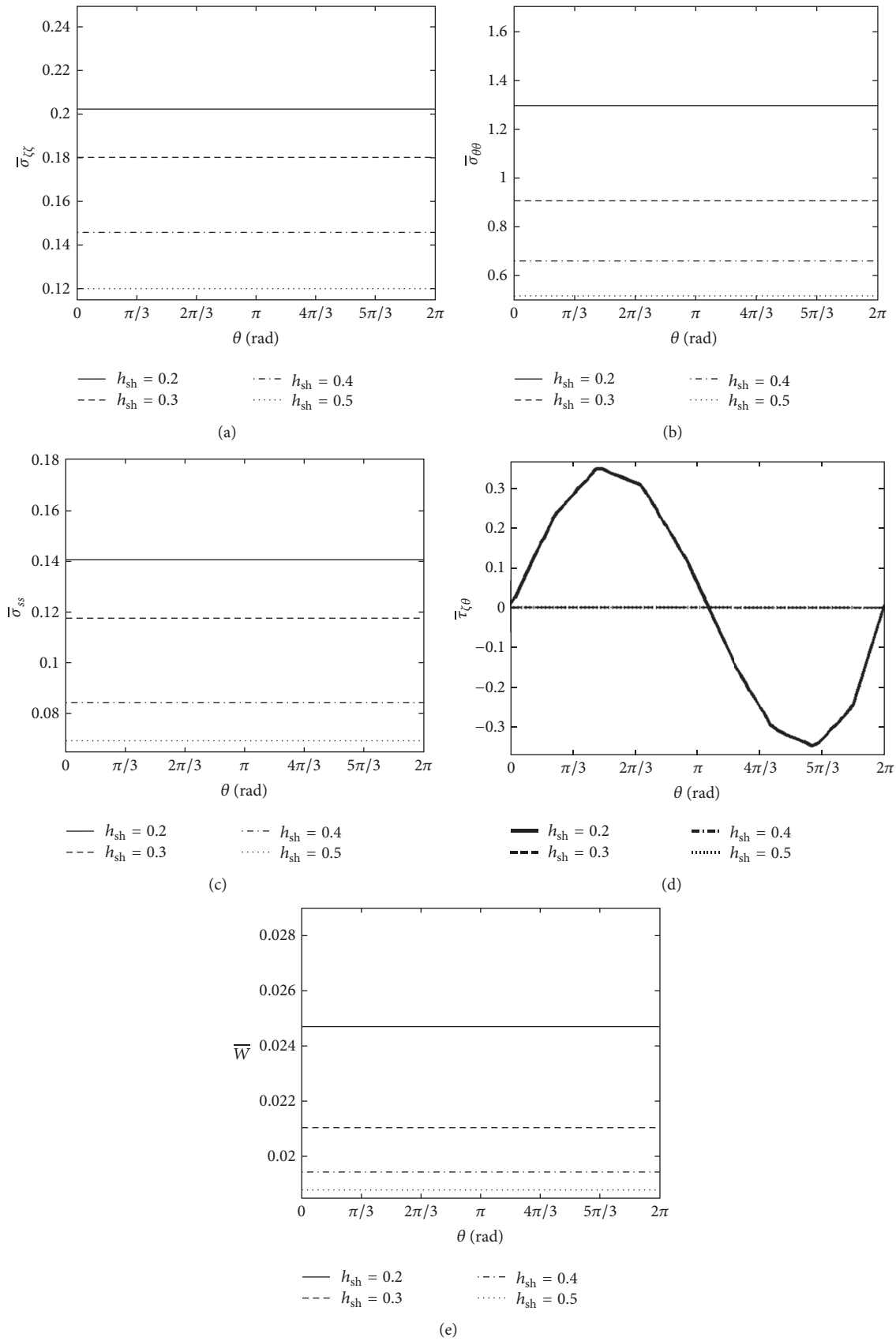

Figure 9: (a) The influence of shell thickness on the stress component in ζ direction through circumferential distribution. (b) The influence of shell thickness on the stress component in θ direction through circumferential distribution. (c) The influence of shell thickness on the stress component in s direction through circumferential distribution. (d) The influence of shell thickness on the shear stress through circumferential distribution. (e) The influence of shell thickness on the displacement component in ζ direction, through circumferential distribution.

constant n changed from 1 to 3. It was also concluded that, by controlling FG in-homogeneity constant n, the values of stresses can be reduced and, consequently, contribute to lessen the failure-susceptibility and progressive rupture in components.

(2) As temperature gradient through thickness increased, the magnitudes of thickness stress and displacement were augmented.

(3) Changing the boundary conditions at edge from the clamped to simply supported caused reduction of the values of stress components and displacement.

(B) Asymmetric loading and boundary conditions:

(1) Stress components and displacement values increased as rotating angular speed increased.

(2) Increasing temperature gradient though thickness caused increase in the thickness stress and thickness displacement, whereas the circumferential variations of hoop stress and also stress in generator direction decreased.

(3) It can be inferred from the plotted results that the shell thickness has pronounced effects on the stresses and thickness displacement that, by increasing the shell thickness, the amplitudes of the thermoelastic parameters decreased.

Appendix

DQ form of (7a) is as follows:

$$\begin{aligned}
&\frac{E_0\left(1+\zeta_i/h_{\mathrm{sh}}\right)^n}{(1+\upsilon)(1-2\upsilon)}\left((1-\upsilon)\left(\sum_{n=1}^{P}C^{(2)}{}_{kn}u_{ijn}\right)\right.\\
&\quad+\upsilon\left(\left(\sum_{l=1}^{N}\sum_{n=1}^{P}A^{(1)}{}_{il}C^{(1)}{}_{kn}w_{ljn}\right)\right.\\
&\quad+Z^2\left(\left(\sum_{m=1}^{M}B^{(1)}{}_{jm}v_{imk}\right)\sin(\gamma)+u_{ijk}\sin^2(\gamma)+w_{ijk}\right.\\
&\quad\cdot\sin(\gamma)\cos(\gamma)\\
&\quad-2\left(\left(\sum_{m=1}^{M}B^{(1)}{}_{jm}v_{imk}\right)+u_{ijk}\sin(\gamma)+w_{ijk}\cos(\gamma)\right)\\
&\quad\cdot\sin(\gamma)\Big)+Z\left(\left(\sum_{m=1}^{M}\sum_{n=1}^{P}B^{(1)}{}_{jm}C^{(1)}{}_{kn}v_{imn}\right)\right.\\
&\quad+\left(\sum_{n=1}^{P}C^{(1)}{}_{kn}u_{ijn}\right)\sin(\gamma)+\left(\sum_{n=1}^{P}C^{(1)}{}_{kn}w_{ijn}\right)\\
&\quad\cdot\cos(\gamma)\Big)\Big)\Big)+\frac{E_0\left(1+\zeta_i/h_{\mathrm{sh}}\right)^n}{2(1+\upsilon)}\left(\left(\sum_{l=1}^{N}A^{(2)}{}_{il}u_{ljk}\right)\right.\\
&\quad+\left(\sum_{l=1}^{N}\sum_{n=1}^{P}A^{(1)}{}_{il}C^{(1)}{}_{kn}w_{ljn}\right)\\
&\quad+\frac{n\left(\left(\sum_{l=1}^{N}A^{(1)}{}_{il}u_{ljk}\right)+\left(\sum_{n=1}^{P}C^{(1)}{}_{kn}w_{ijn}\right)\right)}{h_{\mathrm{sh}}\left(1+\zeta/h_{\mathrm{sh}}\right)^n}\\
&\quad+Z\left(2\left(\left(\sum_{n=1}^{P}C^{(1)}{}_{kn}U_{ijn}\right)\right.\right.\\
&\quad-Z\left(\left(\sum_{m=1}^{M}B^{(1)}{}_{jm}v_{imk}\right)+u_{ijk}\sin(\gamma)+w_{ijk}\cos(\gamma)\right)\Big)\\
&\quad\cdot\sin(\gamma)+\left(\left(\sum_{l=1}^{N}A^{(1)}{}_{il}u_{ljk}\right)+\left(\sum_{n=1}^{P}C^{(1)}{}_{kn}w_{ijn}\right)\right.\\
&\quad+\left(\sum_{m=1}^{M}\sum_{n=1}^{P}B^{(1)}{}_{jm}C^{(1)}{}_{kn}v_{imn}\right)\\
&\quad+Z\left(\left(\sum_{m=1}^{M}B^{(2)}{}_{jm}u_{imk}\right)-\left(\sum_{m=1}^{M}B^{(1)}{}_{jm}v_{imk}\right)\sin(\gamma)\right)\Big)\\
&\quad\cdot\cos(\gamma)\Big)\Big)+\rho_0\left(1+\frac{\zeta_i}{h_{\mathrm{sh}}}\right)^n\left(\cos(\gamma)\zeta_i+\sin(\gamma)s_k\right)\omega^2\\
&\quad\cdot\sin(\gamma)=0.
\end{aligned}\tag{A.1}$$

Applied DQ method (7b) is discretized as

$$\begin{aligned}
&\frac{E_0\left(1+\zeta/h_{\mathrm{sh}}\right)^n}{2(1+\upsilon)}\left(\left(\sum_{n=1}^{P}C^{(2)}{}_{kn}v_{ijn}\right)+\left(\sum_{l=1}^{N}A^{(2)}{}_{il}v_{ljk}\right)+\frac{n\left(Z\left(\left(\sum_{m=1}^{M}B^{(1)}{}_{jm}w_{imk}\right)-v_{ijk}\cos(\gamma)\right)+\left(\sum_{l=1}^{N}A^{(1)}{}_{il}v_{ljk}\right)\right)}{h_{\mathrm{sh}}\left(1+\zeta/h_{\mathrm{sh}}\right)^n}\right.\\
&\quad+Z^2\left(\left(v_{ijk}\sin(\gamma)-\left(\sum_{m=1}^{M}B^{(1)}{}_{jm}u_{imk}\right)\right)\sin(\gamma)+\left(v_{ijk}\cos(\gamma)-\left(\sum_{m=1}^{M}B^{(1)}{}_{jm}w_{imk}\right)\right)\cos(\gamma)\right)\\
&\quad+Z\left(\left(\sum_{m=1}^{M}\sum_{n=1}^{P}B^{(1)}{}_{jm}C^{(1)}{}_{kn}u_{imn}\right)-\left(\sum_{n=1}^{P}C^{(1)}{}_{kn}v_{ijn}\right)\sin(\gamma)+\left(\sum_{l=1}^{N}\sum_{m=1}^{M}A^{(1)}{}_{il}B^{(1)}{}_{jm}w_{lmk}\right)-\left(\sum_{l=1}^{N}A^{(1)}{}_{il}v_{ljk}\right)\cos(\gamma)\right)\\
&\quad+\frac{ZE_0\left(1+\zeta/h_{\mathrm{sh}}\right)^n}{(1+\upsilon)(1-2\upsilon)}\left((1-\upsilon)\left(Z\left(\left(\sum_{m=1}^{M}B^{(2)}{}_{jm}v_{imk}\right)+\left(\sum_{m=1}^{M}B^{(1)}{}_{jm}u_{imk}\right)\sin(\gamma)+\left(\sum_{m=1}^{M}B^{(1)}{}_{jm}w_{imk}\right)\cos(\gamma)\right)\right)\right.
\end{aligned}$$

$$+ \upsilon\left(\left(\sum_{m=1}^{M}\sum_{n=1}^{P} B^{(1)}{}_{jm} C^{(1)}{}_{kn} u_{imn}\right) + \left(\sum_{l=1}^{N}\sum_{m=1}^{M} A^{(1)}{}_{il} B^{(1)}{}_{jm} w_{lmk}\right)\right) + (1-2\upsilon)$$
$$\cdot\left(\left(\left(\sum_{l=1}^{N} A^{(1)}{}_{il} v_{ljk}\right) + Z\left(\left(\sum_{m=1}^{M} B^{(1)}{}_{jm} w_{imk}\right) - v_{ijk}\cos(\gamma)\right)\right)\cos(\gamma)\right.$$
$$\left.+\left(\left(\sum_{n=1}^{P} C^{(1)}{}_{kn} v_{ijn}\right) + Z\left(\left(\sum_{m=1}^{M} B^{(1)}{}_{jm} u_{imk}\right) - v_{ijk}\sin(\gamma)\right)\right)\sin(\gamma)\right) = 0. \tag{A.2}$$

DQ form of (7c) is as follows:

$$\frac{E_0\left(1+\zeta_i/h_{\mathrm{sh}}\right)^n}{2(1+\upsilon)}\left(\left(\sum_{l=1}^{N}\sum_{n=1}^{P} A^{(1)}{}_{il} C^{(1)}{}_{kn} u_{ljn}\right) + \left(\sum_{n=1}^{P} C^{(2)}{}_{kn} w_{ijn}\right)\right)$$
$$+ \frac{E_0\left(1+\zeta_i/h_{\mathrm{sh}}\right)^n n}{h_{\mathrm{sh}}\left(1+\zeta_i/h_{\mathrm{sh}}\right)^n(1+\upsilon)(1-2\upsilon)}\left((1-\upsilon)\right.$$
$$\cdot\left(\sum_{l=1}^{N} A^{(1)}{}_{il} w_{ljk}\right) + \upsilon\left(\left(\sum_{n=1}^{P} C^{(1)}{}_{kn} u_{ijn}\right)\right.$$
$$+ Z\left(\left(\sum_{m=1}^{M} B^{(1)}{}_{jm} v_{imk}\right) + u_{ijk}\sin(\gamma)\right.$$
$$\left.\left.+ w_{ijk}\cos(\gamma)\right)\right) - (1+\upsilon)\alpha\left(1+\frac{\zeta_i}{h_{\mathrm{sh}}}\right)^n T_{ijk}\Bigg)$$
$$+ \frac{E_0\left(1+\zeta_i/h_{\mathrm{sh}}\right)^n}{(1+\upsilon)(1-2\upsilon)}\left((1-\upsilon)\left(\sum_{l=1}^{N} A^{(2)}{}_{il} w_{ljk}\right)\right.$$
$$+ \upsilon\left(\left(\sum_{l=1}^{N}\sum_{n=1}^{P} A^{(1)}{}_{il} C^{(1)}{}_{kn} u_{ljn}\right)\right.$$
$$+ Z^2\left(\left(\sum_{m=1}^{M} B^{(1)}{}_{jm} v_{imk}\right)\cos(\gamma) + u_{ijk}\sin(\gamma)\right.$$
$$\cdot\cos(\gamma) + w_{ijk}\cos^2(\gamma) - 2\left(\left(\sum_{m=1}^{M} B^{(1)}{}_{jm} v_{imk}\right)\right.$$
$$\left.\left.+ u_{ijk}\sin(\gamma) + w_{ijk}\cos(\gamma)\right)\cos(\gamma)\right)$$
$$+ Z\left(\left(\sum_{l=1}^{N}\sum_{m=1}^{M} A^{(1)}{}_{il} B^{(1)}{}_{jm} v_{lmk}\right)\right.$$
$$\left.+\left(\sum_{l=1}^{N} A^{(1)}{}_{il} u_{ljk}\right)\sin(\gamma)\right)$$
$$+\left(\sum_{l=1}^{N} A^{(1)}{}_{il} w_{ljk}\right)\cos(\gamma)\Bigg)\Bigg) - (1+\upsilon)$$
$$\cdot\left(\frac{\alpha\left(1+\zeta_i/h_{\mathrm{sh}}\right)^n m_3 T_{ijk}}{h_{\mathrm{sh}}\left(1+\zeta/h_{\mathrm{sh}}\right)^n} + \alpha\left(1+\frac{\zeta_i}{h_{\mathrm{sh}}}\right)^n\right.$$
$$\left.\cdot\left(\sum_{l=1}^{N} A^{(1)}{}_{il} T_{ljk}\right)\right)\Bigg)$$
$$+ \frac{ZE_0\left(1+\zeta_i/h_{\mathrm{sh}}\right)^n}{2(1+\upsilon)}\left(\left(\sum_{l=1}^{N}\sum_{m=1}^{M} A^{(1)}{}_{il} B^{(1)}{}_{jm} v_{lmk}\right)\right.$$
$$+\left(\left(\sum_{l=1}^{N} A^{(1)}{}_{il} u_{ljk}\right) + \left(\sum_{n=1}^{P} C^{(1)}{}_{kn} w_{ijn}\right)\right)\sin(\gamma)$$
$$+ Z\left(\left(\sum_{m=1}^{M} B^{(2)}{}_{jm} w_{imk}\right) - \left(\sum_{m=1}^{M} B^{(1)}{}_{jm} v_{imk}\right)\right)$$
$$\cdot\cos(\gamma)\Bigg) + 2\left(\left(\sum_{l=1}^{N} A^{(1)}{}_{il} w_{ljk}\right)\right.$$
$$- Z\left(\left(\sum_{m=1}^{M} B^{(1)}{}_{jm} v_{imk}\right) + u_{ijk}\sin(\gamma)\right.$$
$$\left.\left.+ w_{ijk}\cos(\gamma)\right)\right)\cos(\gamma)\Bigg) + \rho_0\left(1+\frac{\zeta_i}{h_{\mathrm{sh}}}\right)^n$$
$$\cdot\left(\cos(\gamma)\zeta_i + \sin(\gamma)s_k\right)\omega^2\cos(\gamma) = 0. \tag{A.3}$$

Discretized form of boundary conditions is as follows:

$$\sigma_{\zeta\zeta} = \frac{E_0\left(1+\zeta_i/h_{\mathrm{sh}}\right)^n(\upsilon)}{(1+\upsilon)(1-2\upsilon)}\left(\left(\sum_{m=1}^{M} C^{(1)}{}_{j,m} u_{j,m,k}\right)\right.$$
$$\left.+ 0.5\left(\sum_{m=1}^{M} C^{(1)}{}_{j,m} w_{j,m,k}\right)^2 - \alpha_0\left(1+\frac{\zeta_i}{h_{\mathrm{sh}}}\right)^n T_{i,j,k}\right)$$
$$+ \frac{E_0\left(1+\zeta_i/h_{\mathrm{sh}}\right)^n(\upsilon)}{(1+\upsilon)(1-2\upsilon)}\left(\left(Z^2\left(\cos(\gamma)\sin(\gamma)u_{i,j,k}w_{i,j,k}\right.\right.\right.$$
$$\left.\left.\left.+ 0.5\left(\cos(\gamma)^2 {w_{i,j,k}}^2 + \sin(\gamma)^2\left({u_{i,j,k}}^2 + {v_{i,j,k}}^2\right)\right) + \sin(\gamma)\right.\right.\right.$$

$$\cdot\left(u_{i,j,k}\left(\sum_{m=1}^{M}C^{(1)}{}_{j,m}v_{j,m,k}\right)-v_{i,j,k}\left(\sum_{m=1}^{M}C^{(1)}{}_{j,m}u_{j,m,k}\right)\right)$$
$$+\cos(\gamma)$$
$$\cdot\left(w_{i,j,k}\left(\sum_{m=1}^{M}C^{(1)}{}_{j,m}v_{j,m,k}\right)-v_{i,j,k}\left(\sum_{m=1}^{M}C^{(1)}{}_{j,m}w_{j,m,k}\right)\right)\Bigg)$$
$$+Z\left(\left(\sum_{m=1}^{M}C^{(1)}{}_{j,m}v_{j,m,k}\right)+w_{i,j,k}\cos(\gamma)+u_{i,j,k}\sin(\gamma)\right)\Bigg)$$
$$-\alpha_0\left(1+\frac{\zeta_i}{h_{\mathrm{sh}}}\right)^n T_{i,j,k}\Bigg)$$
$$+\frac{E_0\left(1+\zeta_i/h_{\mathrm{sh}}\right)^n(1-\upsilon)}{(1+\upsilon)(1-2\upsilon)}\left(\left(\sum_{n=1}^{N}A^{(1)}{}_{k,n}w_{i,j,n}\right)\right.$$
$$\left.+0.5\left(\sum_{n=1}^{N}A^{(1)}{}_{k,n}w_{i,j,n}\right)^2-\alpha_0\left(1+\frac{\zeta_i}{h_{\mathrm{sh}}}\right)^n T_{i,j,k}\right)=0,$$

$$\tau_{\zeta\theta}=\frac{E_0\left(1+\zeta_i/h_{\mathrm{sh}}\right)^n}{2(1+\upsilon)}\left(Z\left(\left(\cos(\gamma)\,w_{i,j,k}+\sin(\gamma)\,u_{i,j,k}\right)\right.\right.$$
$$\cdot\left(\sum_{n=1}^{N}A^{(1)}{}_{k,n}v_{i,j,n}\right)+\left(\left(\sum_{l=1}^{P}B^{(1)}{}_{i,l}w_{l,j,k}\right)-\cos(\gamma)\,v_{i,j,k}\right)$$
$$\cdot\left(\sum_{n=1}^{N}A^{(1)}{}_{k,n}w_{i,j,n}\right)-\cos(\gamma)\,v_{i,j,k}-\left(\sum_{n=1}^{N}A^{(1)}{}_{k,n}u_{i,j,n}\right)$$
$$\left.\left.\cdot\sin(\gamma)\,v_{i,j,k}+\left(\sum_{l=1}^{P}B^{(1)}{}_{i,l}w_{l,j,k}\right)\right)+\left(\sum_{n=1}^{N}A^{(1)}{}_{k,n}v_{i,j,n}\right)\right)$$
$$=0,$$

$$\tau_{s\varsigma}=\frac{E_0\left(1+\zeta_i/h_{\mathrm{sh}}\right)^n}{2(1+\upsilon)}\left(\left(\sum_{n=1}^{N}A^{(1)}{}_{k,n}u_{i,j,n}\right)+\left(\sum_{l=1}^{P}B^{(1)}{}_{i,l}w_{l,j,k}\right)\right.$$
$$\left.+\left(\sum_{l=1}^{P}B^{(1)}{}_{i,l}w_{l,j,k}\right)\left(\sum_{n=1}^{N}A^{(1)}{}_{k,n}w_{i,j,n}\right)\right)=0. \tag{A.4}$$

DQ form of steady-state heat conduction in designated conical coordinate is as follows:

$$\left(\frac{\left(K_0\left(1+\zeta_i/h_{\mathrm{sh}}\right)^n\cos(\gamma)\right)}{(R_1+1/Z)}\right)\left(\sum_{n=1}^{N}A^{(1)}_{i,n}T_{n,j}\right)$$
$$+K_0\left(1+\frac{\zeta_i}{h_{\mathrm{sh}}}\right)^n\left(\sum_{n=1}^{N}A^{(2)}_{i,n}T_{n,j}\right) \tag{A.5}$$
$$+K_0\frac{n}{h}\left(1+\frac{\zeta_i}{h_{\mathrm{sh}}}\right)^{n-1}\left(\sum_{n=1}^{N}A^{(1)}_{i,n}T_{n,j}\right)=0.$$

Nomenclature

f_{Cb}: Centrifugal body force
u, v and w: Displacement components in s, θ and ζ, respectively
L_1: Distance between the origin and the top surface of the cone
L: Length of the generator of the cone
R_1 and R_2: Inner radii of the cone at its small and large ends, respectively
h_{sh}: Thickness of the shell
$A^{(m)}$, $B^{(m)}$ and $C^{(m)}$: Weighting coefficients of the mth derivative along the
E: Elastic constant
ε_{ij}: Strain components.

Greek Symbols

K: Coefficient of heat conductivity
υ: Poisson's ratio
ω: Rotating angular speed
α: Coefficient of thermal expansion
σ_{ij}, τ_{ij}: Components of normal and shear stress tensor
ρ: Density
λ and G: Lame's constants
γ: Semivertex of the conical shell.

Subscripts

n: Power law index
N, M and P: Number of grid points along the thickness, circumferential, and generator directions, respectively.

Conflicts of Interest

The authors declare that they have no conflicts of interest.

References

[1] B. Kieback, A. Neubrand, and H. Riedel, "Processing techniques for functionally graded materials," *Materials Science and Engineering: A Structural Materials: Properties, Microstructure and Processing*, vol. 362, no. 1-2, pp. 81–106, 2003.
[2] A. M. Afsar and J. Go, "Finite element analysis of thermoelastic field in a rotating FGM circular disk," *Applied Mathematical Modelling*, vol. 34, no. 11, pp. 3309–3320, 2010.
[3] M. Bayat, B. B. Sahari, M. Saleem, A. Ali, and S. V. Wong, "Thermoelastic solution of a functionally graded variable thickness rotating disk with bending based on the first-order shear deformation theory," *Thin-Walled Structures*, vol. 47, no. 5, pp. 568–582, 2009.
[4] X.-L. Peng and X.-F. Li, "Thermal stress in rotating functionally graded hollow circular disks," *Composite Structures*, vol. 92, no. 8, pp. 1896–1904, 2010.
[5] K. Kiani, "Thermo-mechanical analysis of functionally graded plate-like nanorotors: A surface elasticity model," *International Journal of Mechanical Sciences*, vol. 106, pp. 39–49, 2016.
[6] V. R. Kar and S. K. Panda, "Nonlinear thermomechanical deformation behaviour of P-FGM shallow spherical shell panel," *Chinese Journal of Aeronautics*, 2015.
[7] M. R. Eslami, M. H. Babaei, and R. Poultangari, "Thermal and mechanical stresses in a functionally graded thick sphere," *International Journal of Pressure Vessels and Piping*, vol. 82, no. 7, pp. 522–527, 2005.

[8] M. Hosseini and A. Dini, "Magneto-thermo-elastic response of a rotating functionally graded cylinder," *Structural Engineering and Mechanics*, vol. 56, no. 1, pp. 137–156, 2015.

[9] S. Natarajan, A. J. Ferreira, S. Bordas, E. Carrera, M. Cinefra, and A. M. Zenkour, "Analysis of functionally graded material plates using triangular elements with cell-based smoothed discrete shear gap method," *Mathematical Problems in Engineering*, Article ID 247932, Art. ID 247932, 13 pages, 2014.

[10] S.-Y. Leu and L.-C. Chien, "Thermoelastic analysis of functionally graded rotating disks with variable thickness involving non-uniform heat source," *Journal of Thermal Stresses*, vol. 38, no. 4, pp. 415–426, 2015.

[11] A. Mehditabar, R. Akbari Alashti, and M. H. Pashaei, "Magneto-thermo-elastic analysis of a functionally graded conical shell," *Steel and Composite Structures*, vol. 16, no. 1, pp. 79–98, 2014.

[12] D. Punera, T. Kant, and Y. M. Desai, "Thermoelastic analysis of laminated and functionally graded sandwich cylindrical shells with two refined higher order models," *Journal of Thermal Stresses*, vol. 41, no. 1, pp. 54–79, 2018.

[13] L. Xin, G. Dui, S. Yang, and D. Zhou, "Solutions for behavior of a functionally graded thick-walled tube subjected to mechanical and thermal loads," *International Journal of Mechanical Sciences*, vol. 98, pp. 70–79, 2015.

[14] T. Prakash and M. Ganapathi, "Asymmetric flexural vibration and thermoelastic stability of FGM circular plates using finite element method," *Composites Part B: Engineering*, vol. 37, no. 7-8, pp. 642–649, 2006.

[15] R. Kumar, N. Sharma, and P. Lata, "Thermomechanical interactions in transversely isotropic magnetothermoelastic medium with vacuum and with and without energy dissipation with combined effects of rotation, vacuum and two temperatures," *Applied Mathematical Modelling: Simulation and Computation for Engineering and Environmental Systems*, vol. 40, no. 13-14, pp. 6560–6575, 2016.

[16] S. A. Hosseini Kordkheili and M. Livani, "Thermoelastic creep analysis of a functionally graded various thickness rotating disk with temperature-dependent material properties," *International Journal of Pressure Vessels and Piping*, vol. 111-112, pp. 63–74, 2013.

[17] M. Saadatfar and M. Aghaie-Khafri, "Thermoelastic analysis of a rotating functionally graded cylindrical shell with functionally graded sensor and actuator layers on an elastic foundation placed in a constant magnetic field," *Journal of Intelligent Material Systems and Structures*, vol. 27, no. 4, pp. 512–527, 2016.

[18] A. N. Eraslan and T. Akis, "Plane strain analytical solutions for a functionally graded elastic-plastic pressurized tube," *International Journal of Pressure Vessels and Piping*, vol. 83, no. 9, pp. 635–644, 2006.

[19] M. Jabbari, M. Z. Nejad, and M. Ghannad, "Thermo-elastic analysis of axially functionally graded rotating thick cylindrical pressure vessels with variable thickness under mechanical loading," *International Journal of Engineering Science*, vol. 96, pp. 1–18, 2015.

[20] A. Chikh, A. Bakora, H. Heireche, M. S. A. Houari, A. Tounsi, and E. A. Adda Bedia, "Thermo-mechanical postbuckling of symmetric S-FGM plates resting on Pasternak elastic foundations using hyperbolic shear deformation theory," *Structural Engineering and Mechanics*, vol. 57, no. 4, pp. 617–639, 2016.

[21] A. Behravan Rad, "Thermo-elastic analysis of functionally graded circular plates resting on a gradient hybrid foundation," *Applied Mathematics and Computation*, vol. 256, pp. 276–298, 2015.

[22] S. Isavand, M. Bodaghi, M. Shakeri, and J. A. Mohandesi, "Dynamic response of functionally gradient austenitic-ferritic steel composite panels under Thermo-mechanical loadings," *Steel and Composite Structures*, vol. 18, no. 1, pp. 1–28, 2015.

[23] A. Mehditabar, "Three-dimensional Magneto-thermo-elastic Analysis of Functionally Graded Truncated Conical Shells," *International Journal of Engineering*, vol. 26, no. 12 (C), 2012.

[24] M. Jabbari, S. Sohrabpour, and M. R. Eslami, "Mechanical and thermal stresses in a functionally graded hollow cylinder due to radially symmetric loads," *International Journal of Pressure Vessels and Piping*, vol. 79, no. 7, pp. 493–497, 2002.

[25] T. Chung, *General continuum mechanics*, Cambridge University Press, 1988.

[26] R. Akbari Alashti, M. Khorsand, and M. H. Tarahhomi, "Three-dimensional asymmetric thermo-elastic analysis of a functionally graded rotating cylindrical shell," *Journal of Theoretical and Applied Mechanics*, vol. 51, no. 1, pp. 143–158, 2013.

[27] C. Shu, *Differential Quadrature and Its Application in Engineering*, Science & Business Media, Springer, 2012.

[28] M. Higuchi, R. Kawamura, Y. Tanigawa, and H. Fujieda, "Magnetothermoelastic stresses induced by a transient magnetic field in an infinite conducting plate," *Journal of Mechanics of Materials and Structures*, vol. 2, no. 1, pp. 113–130, 2007.